molecular pharmaceutics

Article

pubs.acs.org/molecularpharmaceutics

^{99m}Tc-Galacto-RGD$_2$: A Novel ^{99m}Tc-Labeled Cyclic RGD Peptide Dimer Useful for Tumor Imaging

Shundong Ji,[†] Andrzej Czerwinski,*[,‡] Yang Zhou,[†] Guoqiang Shao,[†] Francisco Valenzuela,[‡] Paweł Sowiński,[§] Satendra Chauhan,[‡] Michael Pennington,[‡] and Shuang Liu*[,†]

[†]School of Health Sciences, Purdue University, West Lafayette, Indiana 47907, United States

[‡]Peptides International, Inc., Louisville, Kentucky 40299, United States

[§]Gdańsk University of Technology, 80-233 Gdańsk, Poland

Supporting Information

ABSTRACT: This study sought to evaluate [^{99m}Tc(HYNIC-Galacto-RGD$_2$)-(tricine)(TPPTS)] (^{99m}Tc-Galacto-RGD$_2$: HYNIC = 6-hydrazinonicotinyl; Galacto-RGD$_2$ = Glu[cyclo[Arg-Gly-Asp-D-Phe-Lys(SAA-PEG$_2$-(1,2,3-triazole)-1-yl-4-methyl-amide)]]$_2$ (SAA = 7-amino-L-glycero-L-galacto-2,6-anhydro-7-deoxyheptanamide, and PEG$_2$ = 3,6-dioxaoctanoic acid); and TPPTS = trisodium triphenylphosphine-3,3′,3″-trisulfonate) as a new radiotracer for tumor imaging. Galacto-RGD$_2$ was prepared via the copper(I)-catalyzed 1,3-dipolar azide−alkyne Huisgen cycloaddition. HYNIC-Galacto-RGD$_2$ was prepared by reacting Galacto-RGD$_2$ with sodium succinimidyl 6-(2-(2-sulfonatobenzaldehyde)hydrazono)nicotinate (HYNIC-OSu) in the presence of diisopropylethylamine, and was evaluated for its integrin $\alpha_v\beta_3$ binding affinity against ^{125}I-echistatin bound to U87MG glioma cells. The IC$_{50}$ value for HYNIC-Galacto-RGD$_2$ was determined to be 20 ± 2 nM. ^{99m}Tc-Galacto-RGD$_2$ was prepared in high specific activity (~185 GBq/μmol) and high radiochemical purity (>95%), and was evaluated in athymic nude mice bearing U87MG glioma xenografts for its tumor-targeting capability and biodistribution. The tumor uptake of ^{99m}Tc-Galacto-RGD$_2$ was 10.30 ± 1.67, 8.37 ± 2.13, 6.86 ± 1.33, and 5.61 ± 1.52%ID/g at 5, 30, 60, and 120 min p.i., respectively, which was in agreement with high integrin $\alpha_v\beta_3$ expression on glioma cells and neovasculature. Its lower uptake in intestines, lungs, and spleen suggests that ^{99m}Tc-Galacto-RGD$_2$ has advantages over ^{99m}Tc-3P-RGD$_2$ ([^{99m}Tc(HYNIC-3P-RGD$_2$)(tricine)(TPPTS)]: 3P-RGD$_2$ = PEG$_4$-E[PEG$_4$-c(RGDfK)]$_2$; PEG$_4$ = 15-amino-4,7,10,13-tetraoxapentadecanoic acid) for imaging tumors in the chest and abdominal regions. U87MG tumors were readily detected by SPECT and the tumor uptake of ^{99m}Tc-Galacto-RGD$_2$ was integrin $\alpha_v\beta_3$-specific. ^{99m}Tc-Galacto-RGD$_2$ also had very high metabolic stability. On the basis of results from this study, it was concluded that ^{99m}Tc-Galacto-RGD$_2$ is an excellent radiotracer for imaging integrin $\alpha_v\beta_3$-positive tumors and related metastases.

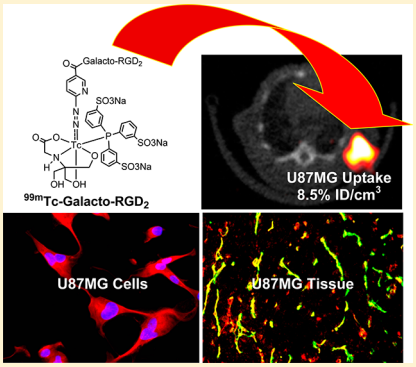

KEYWORDS: *integrin $\alpha_v\beta_3$, ^{99m}Tc-labeling, RGD-containing glycopeptide, tumor imaging, SPECT*

INTRODUCTION

Integrin $\alpha_v\beta_3$ plays a significant role in tumor angiogenesis and metastasis.[1−8] It is a receptor for the extracellular matrix proteins (e.g.vitronectin, fibronectin, fibrinogen, lamin, collagen, von Willibrand factor, and osteoponin) with the exposed arginine-glycine-aspartic (RGD) peptide sequence.[9−11] Integrin $\alpha_v\beta_3$ is expressed at low levels on epithelial cells and mature endothelial cells, but it is overexpressed on activated endothelial cells of neovasculature and some tumor cells. Thus, integrin $\alpha_v\beta_3$ is considered an interesting molecular target for early cancer detection.[12−18]

Cyclic RGD peptides, such as E[c(RGDfK)]$_2$ (Figure 1: RGD$_2$) and E{E[c(RGDfK)]$_2$}$_2$ (RGD$_4$), are potent integrin $\alpha_v\beta_3$ receptor antagonists.[10,11,16,18] Over the last several years, many radiolabeled (^{99m}Tc, ^{18}F, ^{64}Cu, ^{68}Ga and ^{111}In) multimeric cyclic RGD peptides have been evaluated as integrin $\alpha_v\beta_3$-targeted radiotracers for tumor imaging by single photon emission computed tomography (SPECT) or positron emission tomography (PET).[19−39] It was shown that these cyclic RGD peptides were able to bind integrin $\alpha_v\beta_3$ with high specificity.[16,18] Multiple RGD moieties were utilized to maximize their integrin $\alpha_v\beta_3$ binding affinity and the radiotracer tumor uptake.[15,16,18] It was found that radiolabeled multimeric RGD peptides had significantly higher tumor uptake with much longer tumor retention time than their monomeric counterparts.[16,18,24−39] It was also found that cyclic RGD peptide tetramers, such as RGD$_4$, are bivalent in binding to integrin $\alpha_v\beta_3$ even though they have four identical RGD motifs.[36,38]

We have been interested in radiolabeled cyclic RGD peptides as PET or SPECT radiotracers for molecular imaging of solid tumors.[30−44] [^{99m}Tc(HYNIC-3P-RGD$_2$)(tricine)(TPPTS)]

Received: February 15, 2013
Revised: June 10, 2013
Accepted: July 21, 2013
Published: July 22, 2013

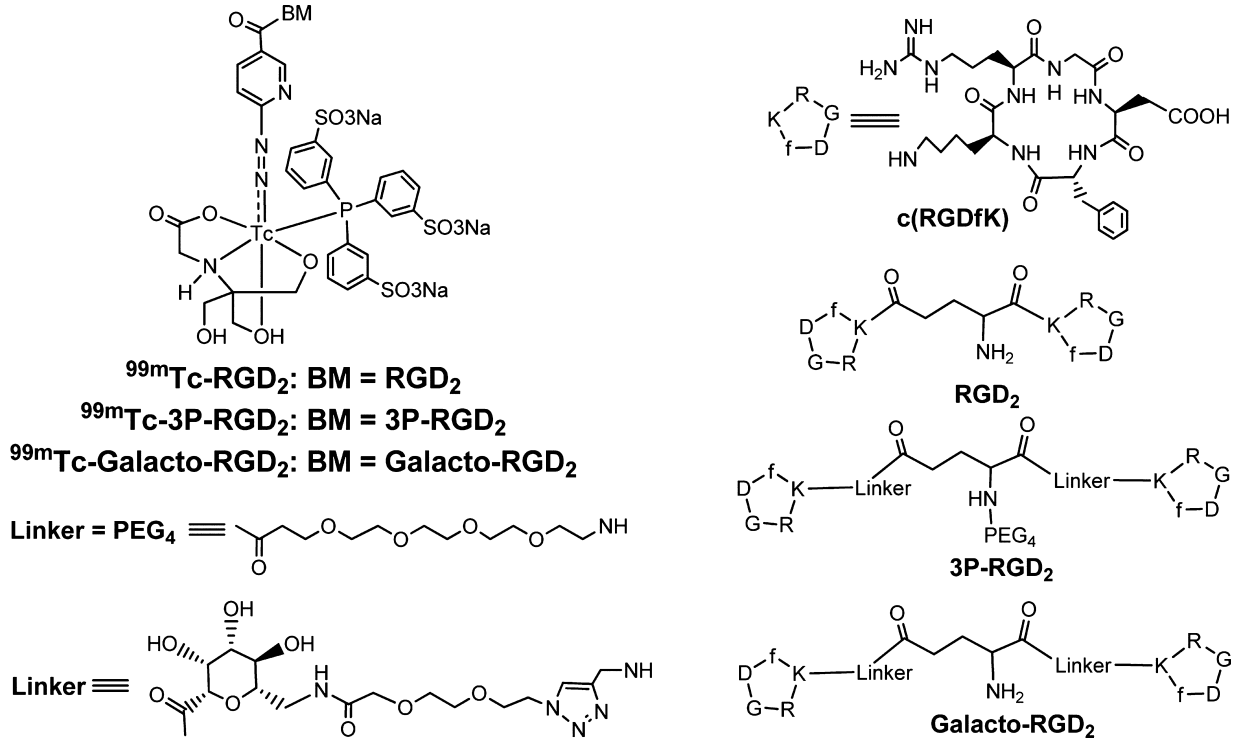

Figure 1. Structures of cyclic RGD peptides (c(RGDfK), RGD_2, 3P-RGD_2, and Galacto-RGD_2) and their corresponding ternary ligand complexes [^{99m}Tc(HYNIC-BM)(tricine)(TPPTS)] (BM = biomolecule); ^{99m}Tc-RGD_2: BM = RGD_2; ^{99m}Tc-3P-RGD_2: BM = 3P-RGD_2, ^{99m}Tc-Galacto-RGD_2: BM = Galacto-RGD_2. The 7-amino-L-glycero-L-galacto-2,6-anhydro-7-deoxyheptanamide (SAA) and 1,2,3-triazole moieties are used to increase the hydrophilicity of ^{99m}Tc-Galacto-RGD_2, and minimize its accumulation in normal organs, such as intestines, lungs, and spleen.

(Figure 1: ^{99m}Tc-3P-RGD_2: HYNIC = 6-hydrazinonicotinyl; 3P-RGD_2 = PEG_4-E[PEG_4-c(RGDfK)]$_2$; PEG_4 = 15-amino-4,7,10,13-tetraoxapentadecanoic acid; and TPPTS = trisodium triphenylphosphine-3,3′,3″-trisulfonate) is a ^{99m}Tc-labeled cyclic RGD peptide dimer.[31] It could be prepared from $^{99m}TcO_4^-$ with high specific activity using a kit formulation.[31,40] ^{99m}Tc-3P-RGD_2 showed very high tumor uptake and rapid renal clearance in glioma-bearing nude mice,[31] and its tumor uptake correlated well linearly with the integrin $\alpha_v\beta_3$ expression levels in five different tumor-bearing small animal models.[42] ^{99m}Tc-3P-RGD_2 SPECT/CT has been successfully used to quantify the tumor uptake and for noninvasive monitoring of progression of breast cancer lung metastases.[43,44] It is currently under clinical investigation as a new radiotracer for tumor imaging in cancer patients.[45,46]

However, ^{99m}Tc-3P-RGD_2 has high uptake in intestines and spleen,[31,45,46] which makes it difficult to image tumors in the abdominal region. To minimize excess radioactivity accumulation in normal organs, we designed and prepared a new cyclic RGD peptide dimer, Galacto-RGD_2 (Figure 1), in which the 7-amino-L-glycero-L-galacto-2,6-anhydro-7-deoxyheptanamide (SAA) groups were used to bridge the two cyclic RGD moieties. SAA has been successfully used to improve pharmacokinetics of ^{18}F-labeled cyclic RGD peptides.[19−21,47] The 1,2,3-triazole moiety was reported to have beneficial effect on pharmacokinetics of radiotracers by increasing their washout efficiency from liver and GI tract.[48] With this in mind, we decided to combine the SAA and 1,2,3-triazole moieties in Galacto-RGD_2. Our hypothesis is that the SAA and 1,2,3-triazole moieties will help to reduce its accumulation in normal organs, such as the intestines, liver, lungs, and spleen.

In this report, we present the synthesis of Galacto-RGD_2, and evaluations of its ^{99m}Tc complex [^{99m}Tc(HYNIC-Galacto-RGD_2)(tricine)(TPPTS)] (Figure 1: ^{99m}Tc-Galacto-RGD_2) as a new radiotracer for tumor imaging. Integrin $\alpha_v\beta_3$ binding affinity of HYNIC-Galacto-RGD_2 was determined in an in vitro displacement assay. Biodistribution properties of ^{99m}Tc-Galacto-RGD_2 were evaluated in the athymic nude mice bearing U87MG glioma xenografts, and compared to those of ^{99m}Tc-3P-RGD_2. The main objective of this study was to demonstrate that SAA and 1,2,3-triazole moieties are indeed able to improve excretion kinetics of ^{99m}Tc radiotracer from noncancerous organs.

■ EXPERIMENTAL SECTION

Materials and Instruments. Chemicals were purchased from Sigma-Aldrich (St. Louis, MO), and were used without purification unless specified. The Boc-protected glutamic acid was purchased from Senn Chemicals (San Diego, CA), and 8-azido-3,6-dioxaoctanoic acid (N_3−PEG_2−OH) was from Peptides International Inc. (Louisville, KY). The protected peptide [cyclo[Arg(Pbf)-Gly-Asp(O*t*Bu)-D-Phe-Lys(SAA)]] (Galacto-RGD) was prepared using the literature procedure.[47] Sodium succinimidyl 6-(2-(2-sulfonatobenzaldehyde)-hydrazono)nicotinate (HYNIC-OSu) was prepared according to the literature method.[49] [^{99m}Tc(HYNIC-3P-RGD_2)(tricine)-(TPPTS)] (^{99m}Tc-3P-RGD_2) was prepared using the procedure described in our previous reports.[31,40] Na$^{99m}TcO_4$ was obtained from Cardinal HealthCare (Chicago, IL). The MALDI (matrix-assisted laser desorption ionization) mass spectral data were collected on an Applied Biosystems Voyager DE PRO mass spectrometer (Framingham, MA), the Department of Chemistry, Purdue University. Melting point was determined on a

dx.doi.org/10.1021/mp400085d | *Mol. Pharmaceutics* 2013, 10, 3304−3314

Buchi B-540 melting point apparatus and was uncorrected. Optical rotation was determined on a DIP-370 polarimeter (Jasco, Easton, MD). Thin layer chromatography was performed using Merck F_{254} silica gel plates (EMD, Darmstadt, Germany). NMR spectra were recorded with a Varian Unity 500 Plus spectrometer (Palo Alto, CA) in DMSO-d_6.

HPLC Methods. The RP-HPLC (Method 1) used a Shimadzu preparative system consisting of two LC-8A pumps controlled by a Shimadzu SCL-10A system, and a Shimadzu UV/vis detector SPD-6A (λ = 220 nm) equipped with a preparative flow cell and a Prochrom preparative HPLC column (50 mm × 35 cm, 100 Å pore size, Phenomenex, Torrance, CA). The flow rate was 100 mL/min with a gradient phase starting from 90% A (0.05% TFA in H_2O) and 10% B (0.05% TFA in CH_3CN) at 0 min to 60% A and 40% B at 60 min. HPLC Method 2 used a LabAlliance HPLC system (Scientific Systems, Inc., State College, PA) equipped with a UV/vis detector (λ = 254 nm) and Zorbax C_{18} column (9.4 mm × 250 mm, 100 Å pore size; Agilent Technologies, Santa Clara, CA). The flow rate was 2.5 mL/min with a mobile phase being 90% A and 10% B at 0 min to 80% A and 20% B at 5 min, and to 70% A and 30% B at 20 min. The radio-HPLC (Method 3) used the LabAlliance HPLC system equipped with a β-ram IN/US detector (Tampa, FL) and Zorbax C_{18} column (4.6 mm × 250 mm, 300 Å pore size; Agilent Technologies, Santa Clara, CA). The flow rate was 1 mL/min. The mobile phase was isocratic for the first 5 min with 90% A (25 mM NH_4OAc, pH = 6.8) and 10% B (acetonitrile), followed by a gradient mobile phase going from 90% A and 10% B at 5 min to 60% A and 40% B at 20 min.

Boc-L-glutamic Acid Bis-propargyl Amide (1). To a solution of Boc-glutamic acid (2.47 g, 10 mmol) and propargylamine hydrochloride (2.11 g, 23 mmol) in DMF (30 mL) were added diphenylphosphoryl azide (DPPA, 5.2 mL, 24 mmol) and triethylamine (Et_3N, 3.2 mL, 23 mmol) at 0 °C under vigorous stirring. The reaction was allowed to proceed overnight at 0 °C. The pH value of the reaction mixture was kept at 7−8 with Et_3N. The reaction mixture was taken into EtOAc (500 mL) and washed with 0.2 N HCl (2 × 200 mL), brine (100 mL), saturated $NaHCO_3$ solution (3 × 200 mL), and brine (2 × 100 mL). After drying over Na_2SO_4, EtOAc was removed to yield 4.16 g of crude product, which upon trituration with hot isopropyl ether afforded a white solid (2.66 g, 82.9%). Rf (EtOAc/hexane/AcOH 2:1:0.01) = 0.20, melting point 146.2−146.5 °C, $[\alpha]_D^{25}$ 10.4° (c = 1, $CHCl_3$). ESI-MS: m/z = 344.2 $[M + Na]^+$; 322.2 $[M + H]^+$. ^1H NMR (DMSO-d_6, chemical shift δ in ppm, and atom labels according to the structure below): δ 8.25 [1H, bt, J = 5.6 Hz, N(1a)-H], 8.24 [1H, bt, J = 5.6 Hz, N(5a)-H], 6.88 [1H, d, J = 8.0 Hz, N(2a)-H], 3.87 [1H, m, C(2)-H], 3.85 [2H, dd, J = 5.6 Hz, J = 2.3 Hz, C(1b)-H_2], 3.82 [2H, dd, J = 5.6 Hz, J = 2.6 Hz, C(5b)-H_2], 3.10 [1H, t, J = 2.3 Hz, C(1d)-H], 3.08 [1H, t, J = 2.6 Hz, C(5d)-H], 2.10 [2H, m, C(4)-H_2], 1.82 [1H, m, C(3)-H_2], 1.67 [1H, m, C(3)-H_2], and 1.37 [9H, s, C(2e)-H_3]. ^{13}C NMR (DMSO-d_6, chemical shift δ in ppm): 171.5 (C-1), 171.2 (C-5), 155.2 (C-2b), 81.2 (C-1c), 81.1 (C-5c), 78.1 (C-2d), 73.0 (C-5d), 72.9 (C-1d), 53.8 (C-2), 31.6 (C-4), 28.2 (C-2e), 27.9 (C-1b), 27.8 (C3 and C-5b). Anal. Calcd for $C_{16}H_{23}N_3O_4$: C, 59.80; H, 7.21; N, 13.08. Found: C, 59.78; H, 7.19; N, 13.00.

Cyclo[Arg(Pbf)-Gly-Asp(O*t*Bu)-D-Phe-Lys(SAA-PEG$_2$-N$_3$)] (2). To a solution of cyclo[Arg(Pbf)-Gly-Asp(O*t*Bu)-D-Phe-Lys(SAA)] (1.10 g, 1.0 mmol) and N_3−PEG_2−OH (0.28 g, 1.48 mmol) in DMF (15 mL) was added DPPA (0.43 mL, 2.0 mmol) at 0 °C with stirring, followed by the addition of Et_3N (0.21 mL, 1.51 mmol). The reaction mixture was kept at 0 °C for 25 h, with occasional adjustments of the pH (7−8) with Et_3N. After the reaction, the mixture was diluted with 0.4 N HCl (100 mL) and extracted with EtOAc (3 × 300 mL). The combined organic extracts were concentrated. The precipitated product was collected by filtration, washed with cold Et_2O, and dried in vacuo to afford 0.81 g of **2** in 63.7% yield as a colorless solid. ESI-MS: m/z = 945.55 $[M + H]^+$ (M = 945.43 calcd. for $[C_{40}H_{59}N_{13}O_{14}]$).

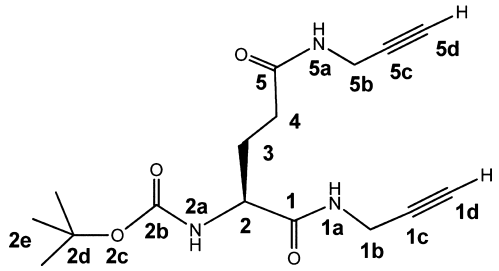

Boc-Glu[cyclo[Arg(Pbf)-Gly-Asp(O*t*Bu)-D-Phe-Lys(SAA-PEG2-(1,2,3-triazole)-1-yl-4-methylamide)]]$_2$ (3). To a stirred solution of **1** (94 mg, 0.29 mmol) and **2** (750 mg, 0.59 mmol) in a mixture of H_2O (2.9 mL) and *t*-BuOH (5.8 mL) were added 1.73 mL of 0.2 M $CuSO_4 \cdot 5H_2O$ and 1.73 mL of 0.5 M sodium ascorbate solution at room temperature. The mixture was stirred for 70 min and then diluted with 60 mL of 1-BuOH and 40 mL of H_2O. The organic layer was washed with H_2O (2 × 30 mL) and concentrated under reduced pressure. Addition of Et_2O resulted in a precipitate, which was collected by filtration, washed with Et_2O, and dried to give 760 mg of **3**. The yield was 91.5%. ESI-MS: m/z = 2249.05 $[M+H]^+$ (M = 2249.05 calcd. for $[C_{96}H_{145}N_{29}O_{34}]$).

H-Glu[cyclo[Arg-Gly-Asp-D-Phe-Lys(SAA-PEG$_2$-(1,2,3-triazole)-1-yl-4-methylamide)]]$_2$ (Galacto-RGD$_2$). The protected Galacto-RGD_2 (750 mg, 0.26 mmol) was dissolved in 20 mL of a solution TFA/TIPS/H_2O (95/2.5/2.5, v/v/v) at room temperature. After 2 h, the reaction mixture was concentrated under reduced pressure. Crude Galacto-RGD_2 was precipitated with cold Et_2O, collected by centrifugation, washed with Et_2O (3 × 30 mL), and dried in vacuo to give 690 mg of white solid, which was purified by RP-HPLC (Method 1) to yield Galacto-RGD_2 (105 mg, 16.2%) as a TFA salt. The HPLC purity was 99.3%. ESI-MS: m/z = 2149.12 $[M+H]^+$ (M = 2149.05 calcd. for $[C_{91}H_{137}N_{29}O_{34}]$).

HYNIC-Glu[cyclo[Arg-Gly-Asp-D-Phe-Lys(SAA-PEG$_2$-(1,2,3-triazole)-1-yl-4-methylamide)]]$_2$ (HYNIC-Galacto-RGD$_2$). HYNIC-OSu (5.4 mg, 12 μmol) and Galacto-RGD_2 (6.5 mg, 3 μmol) were dissolved in DMF (2 mL). After addition of excess diisopropylethylamine (DIEA, 50 μmol), the reaction mixture was stirred for ∼10 days at room temperature. To the reaction mixture was added 2 mL of water after completion of conjugation. The pH value was then adjusted to 3−4 using TFA. The product was separated from the reaction mixture by HPLC (Method 2). Fractions at 14.5 min were collected. Lyophilization of collected fractions afforded HYNIC-Galacto-RGD_2. The yield was 3.5 mg (∼48%). MALDI-MS: m/z = 2452.3 for $[M + H]^+$ (M = 2451.03 calcd. for $[C_{104}H_{146}N_{32}O_{36}S]$).

^{99m}Tc-Labeling. To a lyophilized vial containing 20 μg of HYNIC-Galacto-RGD_2, 7 mg of TPPTS, 6.5 mg of tricine, 40 mg of mannitol, 38.5 mg of disodium succinate hexahydrate, and 12.7 mg of succinic acid was added 1.0−1.5 mL of

$Na^{99m}TcO_4$ solution (~1110 MBq in saline). The reconstituted vial was then heated in a boiling water bath for ~30 min. After radiolabeling, a sample of the resulting solution was analyzed by radio-HPLC (Method 3). The radiochemical purity was >90% for imaging and biodistribution studies. The solution stability was monitored by radio-HPLC for 24 h.

Dose Preparation. For biodistribution, doses were prepared by dissolving ^{99m}Tc-Galacto-RGD_2 in saline to a concentration of ~1 MBq/mL. For SPECT/CT imaging, doses were prepared by dissolving ^{99m}Tc-Galacto-RGD_2 in saline to ~370 MBq/mL. In blocking experiments, RGD_2 was dissolved in the dose solution to 3.5 mg/mL. The resulting dose solution was filtered with a 0.20 μm Millex-LG filter before being injected into animals. Each animal was injected with ~0.1 mL of the dose solution.

Tumor Cell Culture. The U87MG cell line was obtained from ATCC (American Type Culture Collection, Manassas, VA). U87MG cells were cultured in the Minimum Essential Medium, Eagle with Earle's Balanced Salt Solution (non-essential amino acids sodium pyruvate), and were supplemented with 10% fetal bovine serum (FBS, ATCC) and 1% penicillin and streptomycin solution at 37 °C in a humidified atmosphere of 5% CO_2 in air. Cells were grown as monolayers and were harvested or split when they reached 90% confluence to maintain exponential growth.

In Vitro Whole-Cell Integrin $\alpha_v\beta_3$ Binding Assay. The integrin binding affinity of cyclic RGD peptides were assessed via a cellular competitive displacement assay using ^{125}I-echistatin (Perkin-Elmer, Branford, CT) as the integrin-specific radioligand.[31,32] Briefly, the filter multiscreen DV plates (Millipore, Billerica, MA) were seeded with 1×10^5 U87MG cells in binding buffer (20 mM Tris, 150 mM NaCl, 2 mM $CaCl_2$, 1 mM $MnCl_2$, 1 mM $MgCl_2$, 0.1% (w/v) bovine serum albumin; and pH 7.4) and ^{125}I-echistatin (0.75−1.0 kBq) in the presence of increasing concentrations of the cyclic RGD peptide, incubated for 2 h at room temperature. After removing unbound ^{125}I-echistatin, the hydrophilic PVDF filters were washed 3× with the binding buffer, and then collected. Radioactivity was determined using a Perkin-Elmer Wizard 1480 γ-counter (Shelton, CT). Experiments were carried out twice with triplicates. IC_{50} values were calculated by fitting experimental data with nonlinear regression using GraphPad Prism (GraphPad Software, Inc., San Diego, CA), and were reported as an average plus/minus standard deviation.

Animal Models. Biodistribution and imaging studies were performed in compliance with the NIH animal experimentation guidelines (*Principles of Laboratory Animal Care*, NIH Publication No. 86-23, revised 1985). The protocol was approved by the Purdue University Animal Care and Use Committee (PACUC). Female athymic *nu/nu* mice (4−5 weeks) were purchased from Harlan (Indianapolis, IN), and were inoculated subcutaneously with 5×10^6 of U87MG cells into the shoulder flank of each animal. Four weeks after inoculation, the tumor size was 0.1−0.5 g, and animals were used for biodistribution and imaging studies.

Biodistribution Protocol. The tumor-bearing mice (20−25 g) were randomly selected, and each animal was administered with ~0.1 MBq of ^{99m}Tc-Galacto-RGD_2 (~2 ng HYNIC-Galacto-RGD_2) by tail vein injection. Animals (5−8) were sacrificed by sodium pentobarbital overdose (~200 mg/kg) at 5, 30, 60, and 120 min postinjection (p.i.). Blood, tumors, and normal organs (brain, eyes, heart, spleen, lungs, liver, kidneys, muscle, and intestine) were harvested, washed with saline, dried with absorbent tissue, weighed, and counted on a Perkin-Elmer Wizard 1480 γ-counter. The organ uptake was calculated as the percentage of injected dose per gram of wet tissue (%ID/g). The blocking experiment was performed using RGD_2 as the blocking agent in six animals. Each animal was administered with ~0.1 MBq of ^{99m}Tc-Galacto-RGD_2 along with ~350 μg (~14 mg/kg) of RGD_2. Biodistribution data (%ID/g) and tumor-to-background (T/B) ratios were expressed as the average plus standard deviation.

SPECT/CT Imaging. SPECT/CT images were obtained using a u-SPECT-II/CT scanner (Milabs, Utrecht, The Netherlands) equipped with a 0.6 mm multipinhole collimator. The glioma-bearing mouse was injected with ~37 MBq of ^{99m}Tc-Galacto-RGD_2 (~0.8 μg HYNIC-Galacto-RGD_2) in 0.1 mL saline via the tail vein. At 60 min p.i., the animal was placed into a shielded chamber connected to an isoflurane anesthesia unit (Univentor, Zejtun, Malta). Anesthesia was induced using an air flow rate of 350 mL/min and ~3.0% isoflurane. After induction of anesthesia, the animal was immediately placed supine on the scanning bed. The air flow rate was then reduced to ~250 mL/min with ~2.0% isoflurane. Rectangular scan in the regions of interest (ROIs) from SPECT and CT were selected on the basis of orthogonal optical images provided by the integrated webcams. After SPECT acquisition (75 projections over 30 min per frame, 2 frames), the animal was then transferred into the attached CT scanner and imaged using the "normal" acquisition settings (2 degree intervals) at 45 kV and 500 μA. After CT acquisition, the animal was allowed to recover in a lead-shielded cage.

Image Reconstruction and Data Processing. SPECT reconstruction was performed using a POSEM (pixelated ordered subsets by expectation maximization) algorithm with 6 iterations and 16 subsets. CT data were reconstructed using a cone-beam filtered back-projection algorithm (NRecon v1.6.3, Skyscan). After reconstruction, the SPECT and CT data were automatically coregistered according to the movement of the robotic stage, and then resampled to equivalent voxel sizes. Co-registered images were further rendered and visualized using the PMOD software (PMOD Technologies, Zurich, Switzerland). A 3D-Guassian filter (0.8 mm fwhm) was applied to smooth noise, and the LUTs (look up tables) were adjusted for good visual contrast. The reconstructed images were visualized as both orthogonal slices and maximum intensity projections.

Radioactivity Quantification. Radiation sources of known amount of radioactivity were imaged and reconstructed using the same scanning protocol described above. A standard curve was generated to correlate the pixel intensities in the reconstructed images to the radioactivity as measured by a γ-counter. The tumor delineation was performed on CT and SPECT images according to the literature method.[43,44] Briefly, the ROIs (regions of interest) were drawn manually to cover the entire tumor based on transverse view of the CT image. For the tumor delineation with SPECT, a threshold of 50% or more of the maximum pixel value on the SPECT image was chosen. In order to accurately represent the entire tumor, SPECT/CT was also employed to delineate the tumor ROIs. The tumor volume and radioactivity counts were generated by using the PMOD software (PMOD Technologies, Zurich, Switzerland). The amount of radioactivity in each tumor was calculated according to the above-mentioned standard curve. The tumor uptake of ^{99m}Tc-Galacto-RGD_2 was expressed as the percentage of injected dose per unit volume (%ID/cm^3), and was

Chart 1. Syntheses of Galacto-RGD$_2$

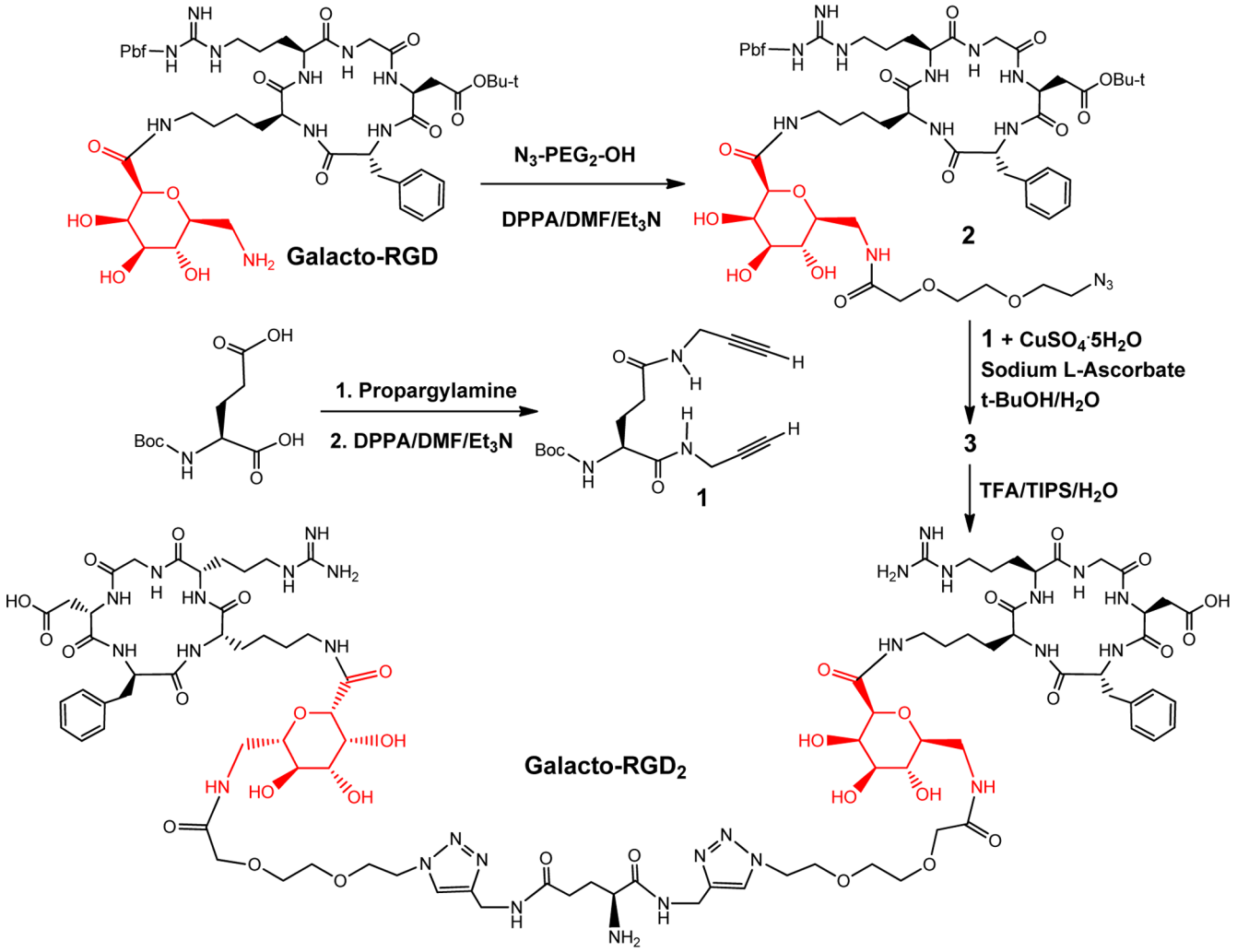

compared with the data from biodistribution in the same tumor-bearing animal model.

Metabolism. Athymic nude mice (n = 3) without tumors were used for metabolism study. Each animal was administered with ~10 MBq of ^{99m}Tc-Galacto-RGD$_2$ via the tail vein. The urine samples were collected at 30 and 120 min p.i. by manual void, and were mixed with equal volume of 50% acetonitrile aqueous solution. The mixture was centrifuged at 8,000 rpm. The supernatant was collected and filtered with a 0.20 μm Millex-LG filter to remove foreign particles. The filtrate was analyzed by HPLC (Method 3). Feces samples were collected at 120 min p.i. and suspended in 20% acetonitrile aqueous solution after homogenization. The resulting mixture was vortexed for ~5 min. After centrifuging at 8000 rpm, the supernatant was collected and filtered with a 0.20 μm Millex-LG filter to remove foreign particles. The filtrate was then analyzed by HPLC (Method 3). The percentage of radioactivity recovery was >95% (by γ-counting) for both urine and feces samples.

Cultured Primary Tumor Cells. The xenografted U87MG tumors were harvested, and were immersed in a growth medium immediately after gamma counting. Tumor tissues were rinsed twice with the Hanks' solution and dissected into small pieces with razor blades. Small tumor pieces were digested with 0.25% Trypsin (1 mM EDTA, without Ca^{2+} and Mg^{2+}) solution at 37 °C for 30 min, followed by vigorous pipetting and filtration through a 40 μm mesh nylon screen. After centrifugation at 1000 rpm for 5 min, the pellet was resuspended in the culture media and incubated at 37 °C in a humidified atmosphere containing 5% CO_2. The purity of tumor cells could reach ~90% after two passages, and the third passage was used for cellular immunostaining studies.

Cellular Immunostaining. The primary U87MG glioma cells were seeded into 8-well chamber slides, and allowed to spread for >24 h. Cells were fixed in −20 °C methanol for 5 min and rinsed with PBS. Cells were incubated in 5% BSA for 30 min to block nonspecific binding, and then added Alexa Fluor 488 conjugated mouse antihuman integrin $\alpha_v\beta_3$ monoclonal antibody LM609 (1:100, Millipore, Billerica, MA) for 1 h at room temperature, or incubated with rabbit antihuman and murine β_3 antibody followed by incubation with Alexa Fluor 594 conjugated goat antirabbit IgG (Santa Cruz, CA). After washing with PBS buffer, the slides were mounted with Dapi-Fluoromount-G (SouthernBiotech, Birmingham, AL). The fluorescence was visualized with an Olympic BX51 microscope (Olympus America Inc., Center Valley, PA).

Tumor Tissue Immunohistochemistry. The U87MG tumors harvested from tumor-bearing mice were immediately snap-frozen in the OCT (optical cutting temperature) solution, and were then cut into slices (5 μm). After thorough drying at

dx.doi.org/10.1021/mp400085d | Mol. Pharmaceutics 2013, 10, 3304−3314

room temperature, slices were fixed with ice-cold acetone for 10 min and then and dried in the air for 20 min. Sections were blocked with 10% goat serum for 30 min at room temperature, and then were incubated with the hamster anti-integrin β_3 antibody (1:100, BD Biosciences, San Jose, CA) and rat anti-CD31 antibody (1:100, BD Biosciences) for 1 h at room temperature. After incubating with the Cy3-conjugated goat anti-hamster and fluorescein isothiocyanate (FITC)-conjugated goat anti-rat secondary antibodies (1:100, Jackson ImmunoResearch Inc., West Grove, PA) and washing with PBS, the fluorescence was visualized with an Olympus fluorescence microscope (Olympus America Inc., Center Valley, PA). All the pictures were taken under 200× magnification with the same exposure time. Brightness and contrast adjustments were made equally to all images.

Statistical Analysis. All experimental data were expressed as the average plus/minus standard deviation. Statistical analysis was performed by one-way analysis of variance (ANOVA) followed by the Newman-Keuls test for multiple comparisons. The level of significance was set at $p < 0.05$.

RESULTS

Synthesis of Galacto-RGD$_2$. Compound **1**, a key intermediate for preparation of Galacto-RGD$_2$, was prepared (Chart 1, ~83% yield) from the reaction of Boc-glutamic acid with two equivalents of propargylamine in the presence of DPPA, which is a coupling agent with low risk of racemization.[50,51] DPPA was also employed in the preparation of **2**. Synthesis of **3** was accomplished in >90% yield by the Cu(I)-catalyzed 1,3-dipolar azide−alkyne Huisgen cycloaddition. It was not necessary to protect the hydroxyl groups in the SAA moieties during this reaction. Deprotection of the Pbf and *t*-butyl protecting groups in **3** under acidic conditions resulted in Galacto-RGD$_2$, which was characterized by HPLC (Figure SI1, Supporting Information), ESI-MS (Figure SI2), and NMR (Figures SI3−SI8: DQF-COSY, NOESY, ROESY, TOCSY, HSQC, and HMBC). The ESI-MS and NMR data (Tables SI1 and SI2) were completely consistent with the structure and composition proposed for Galacto-RGD$_2$.

Synthesis of HYNIC-Galacto-RGD$_2$. HYNIC-Galacto-RGD$_2$ was prepared from the reaction of Galacto-RGD$_2$ with HYNIC-OSu in the presence of excess DIEA. The conjugation reaction was slow, and took about 10 days to complete at room temperature. This was likely due to the fact that the primary amine in Galacto-RGD$_2$ is stereochemically "hindered" by two bulky Galacto-RGD monomers. HYNIC-Galacto-RGD$_2$ was purified by HPLC and characterized by ESI-MS. Its HPLC purity was >95% before being used for ^{99m}Tc-labeling. ESI-MS data was consistent with the proposed composition for HYNIC-Galacto-RGD$_2$.

Integrin $\alpha_v\beta_3$ Binding Affinity. Figure 2 shows the displacement curves of ^{125}I-echistatin bound to U87MG human glioma cells in the presence of HYNIC-Galacto-RGD$_2$. For comparison purposes, we also evaluated c(RGDyK), HYNIC-RGD$_2$, and HYNIC-3P-RGD$_2$ in the same assay. IC$_{50}$ values were calculated to be 20 ± 2, 32 ± 1, 85 ± 2, and 422 ± 15 nM for HYNIC-Galacto-RGD$_2$, HYNIC-3P-RGD$_2$, HYNIC-RGD$_2$, and c(RGDyK), respectively. The IC$_{50}$ values of c(RGDyK) and HYNIC-RGD$_2$ were close to those from our previous report.[31,32] The integrin $\alpha_v\beta_3$ binding affinity follows the rank order of HYNIC-Galacto-RGD$_2$ ≥ HYNIC-3P-RGD$_2$ > HYNIC-RGD$_2$ ≫ c(RGDyK) using the same competitive displacement assay.

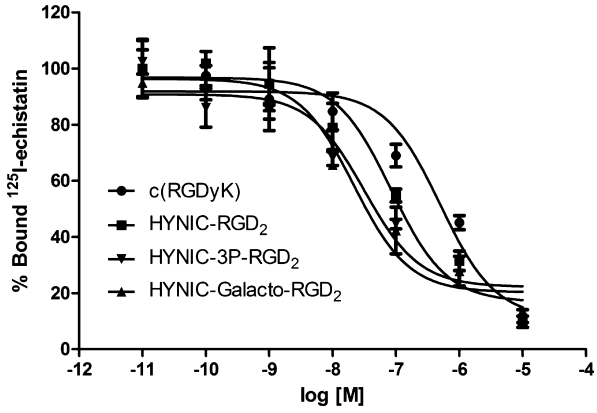

Figure 2. Competitive displacement curves of ^{125}I-echistatin bound to U87MG human glioma cells in the presence of cyclic RGD peptides. HYNIC-3P-RGD$_2$, HYNIC-RGD$_2$, and c(RGDyK) were used for comparison purposes. IC$_{50}$ values were calculated to be 20 ± 2, 32 ± 1, 85 ± 2, and 422 ± 15 nM for HYNIC-Galacto-RGD$_2$, HYNIC-3P-RGD$_2$, HYNIC-RGD$_2$, and c(RGDyK), respectively.

Radiochemistry. ^{99m}Tc-Galacto-RGD$_2$ was prepared from the reaction of HYNIC-Galacto-RGD$_2$ with ^{99m}TcO$_4^-$ in the presence of excess tricine and TPPTS. ^{99m}Tc-labeling was accomplished by heating the reaction mixture at 100 °C for 30 min. Figure 3 shows representative radio-HPLC chromatograms of ^{99m}Tc-Galacto-RGD$_2$ in the kit matrix at 1 and 24 h postlabeling. Its radiochemical purity for was >95% without further chromatographic purification. The specific activity was ~185 GBq/μmol. It remained stable in the kit matrix for more than 24 h postlabeling.

Biodistribution. Table 1 lists the biodistribution data of ^{99m}Tc-Galacto-RGD$_2$ in athymic nude mice bearing U87MG glioma xenografts. Its tumor uptake was 10.30 ± 1.67, 8.37 ± 2.13, 6.86 ± 1.33, and 5.61 ± 1.52%ID/g at 5, 30, 60, and 120 min p.i., respectively. For comparison purposes, we also obtained the 60 min biodistribution data of ^{99m}Tc-3P-RGD$_2$ in the same tumor-bearing animal model. As illustrated in Figure 4A, the tumor uptake of ^{99m}Tc-Galacto-RGD$_2$ was close to that of ^{99m}Tc-3P-RGD$_2$ at <60 min p.i. However, its 120 min tumor uptake (5.61 ± 1.52%ID/g) that was significantly lower than that of ^{99m}Tc-3P-RGD$_2$ (9.74 ± 3.22%ID/g).[31] Replacing PEG$_4$ linkers in ^{99m}Tc-3P-RGD$_2$ with a pair of SAA, 1,2,3-triazole, and PEG$_2$ moieties resulted in faster tumor washout of ^{99m}Tc-Galacto-RGD$_2$. The liver uptake of ^{99m}Tc-Galacto-RGD$_2$ was 4.00 ± 1.10, 2.82 ± 1.25, 3.07 ± 2.14, and 1.54 ± 0.43% ID/g with the tumor/liver ratios being 2.66 ± 0.51, 3.25 ± 0.85, 3.05 ± 1.69, and 4.03 ± 2.04 at 5, 30, 60, and 120 min p.i., respectively. Its liver uptake was comparable to that of ^{99m}Tc-3P-RGD$_2$ over a 2 h period.[31] The main difference between ^{99m}Tc-Galacto-RGD$_2$ and ^{99m}Tc-3P-RGD$_2$ was their uptake in intestines, lungs, and spleen (Figure 4A). For example, the intestine uptake of ^{99m}Tc-Galacto-RGD$_2$ (5.45 ± 1.47%ID/g) was much lower ($p < 0.01$) than that of ^{99m}Tc-3P-RGD$_2$ (9.45 ± 1.31%ID/g) at 60 min p.i.

Integrin $\alpha_v\beta_3$ Specificity. Figure 4B shows the 60 min biodistribution data of ^{99m}Tc-Galacto-RGD$_2$ in athymic nude mice (n = 6) bearing U87MG glioma xenografts in the absence/presence of excess RGD$_2$ (350 μg/mouse or 14 mg/kg). Coinjection of excess RGD$_2$ significantly blocked its tumor uptake (1.48 ± 0.42%ID/g with RGD$_2$ vs 6.86 ± 1.33%ID/g without RGD$_2$). The normal organ uptake was also blocked by coinjection of excess RGD$_2$. For example, the uptake of ^{99m}Tc-

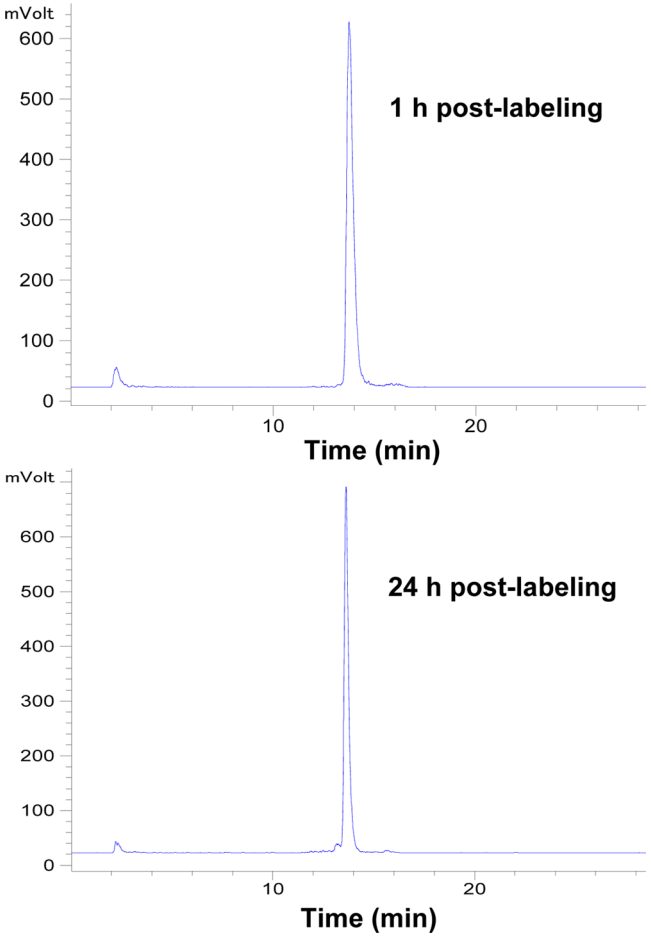

Figure 3. Radio-HPLC chromatograms of ^{99m}Tc-Galacto-RGD$_2$ in the kit matrix at 1 and 24 h postlabeling. The radiometric peak at ~13.5 min was from ^{99m}Tc-Galacto-RGD$_2$. Its radiochemical purity was always >95% without any chromatographic purification.

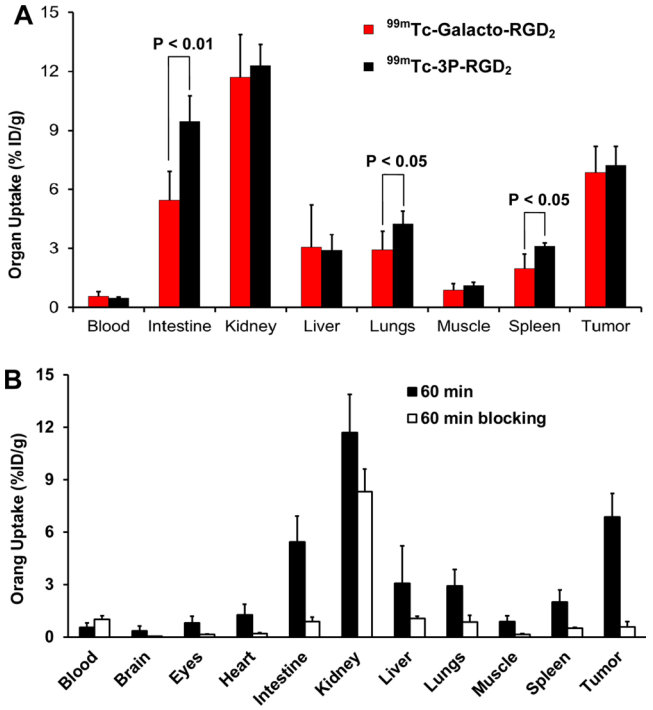

Figure 4. (A) Comparison of the 60 min biodistribution data between ^{99m}Tc-Galacto-RGD$_2$ (n = 8) and ^{99m}Tc-3P-RGD$_2$ (n = 6) in the athymic nude mice bearing U87MG glioma xenografts to demonstrate the advantage of ^{99m}Tc-Galacto-RGD$_2$ over ^{99m}Tc-3P-RGD$_2$. (B) Selected 60 min biodistribution data of ^{99m}Tc-Galacto-RGD$_2$ in the athymic nude mice (n = 8) bearing U87MG glioma xenografts with/without coinjection of RGD$_2$ (350 μg/mouse or 14 mg/kg) to demonstrate its integrin $\alpha_v\beta_3$ specificity.

Galacto-RGD$_2$ in the intestine, lungs, and spleen was 5.56 ± 1.73, 2.19 ± 0.94, and 1.09 ± 0.44%ID/g, respectively, without RGD$_2$, while its uptake in the same organs was 1.82 ± 0.86, 1.52 ± 0.27, and 0.65 ± 0.07%ID/g, respectively, in the presence of RGD$_2$. This experiment clearly demonstrated that the tumor uptake of ^{99m}Tc-Galacto-RGD$_2$ is integrin $\alpha_v\beta_3$-specific.

SPECT/CT Imaging. Figure 5A shows 3D (left) and transverse (right) views of SPECT/CT images of glioma-bearing mice administered with ~37 MBq of ^{99m}Tc-Galacto-

Table 1. Selected Biodistribution Data and Tumor-to-Background Ratios of ^{99m}Tc-Galacto-RGD$_2$ in Athymic Nude Mice Bearing U87MG Human Glioma Xenografts[a]

organ	5 min (n = 5)	30 min (n = 5)	60 min (n = 8)	120 min (n = 8)
blood	1.10 ± 0.16	0.92 ± 0.33	0.56 ± 0.25	0.22 ± 0.03
brain	0.41 ± 0.10	0.22 ± 0.06	0.35 ± 0.28	0.14 ± 0.12
eyes	1.54 ± 0.49	1.20 ± 0.50	0.81 ± 0.39	0.52 ± 0.15
heart	2.36 ± 0.29	1.65 ± 1.10	1.27 ± 0.61	0.56 ± 0.08
intestine	3.78 ± 0.52	4.24 ± 1.54	5.45 ± 1.47	3.37 ± 1.32
kidney	18.75 ± 2.79	13.13 ± 4.75	11.70 ± 4.06	6.04 ± 1.92
liver	4.00 ± 0.10	2.82 ± 1.25	3.07 ± 2.14	1.54 ± 0.43
lungs	5.41 ± 0.58	4.24 ± 1.71	2.93 ± 0.94	1.31 ± 0.23
muscle	2.73 ± 0.89	1.10 ± 0.25	0.88 ± 0.34	0.47 ± 0.12
spleen	2.97 ± 0.43	2.53 ± 0.85	1.99 ± 0.71	1.46 ± 0.26
tumor	10.30 ± 1.67	8.37 ± 2.13	6.86 ± 1.33	5.61 ± 1.52
tumor/blood	9.43 ± 1.19	9.65 ± 2.03	15.94 ± 8.85	26.48 ± 8.71
tumor/kidney	0.52 ± 0.14	0.61 ± 0.12	0.79 ± 0.40	0.89 ± 0.48
tumor/liver	2.66 ± 0.51	3.25 ± 0.85	3.05 ± 1.69	4.03 ± 2.04
tumor/lung	1.90 ± 0.21	2.19 ± 0.75	2.73 ± 1.33	4.38 ± 1.34
tumor/muscle	3.98 ± 0.75	7.97 ± 2.53	9.40 ± 5.11	12.91 ± 4.95

[a]The tumor uptake was expressed as an average plus/minus the standard deviation.

dx.doi.org/10.1021/mp400085d | Mol. Pharmaceutics 2013, 10, 3304−3314

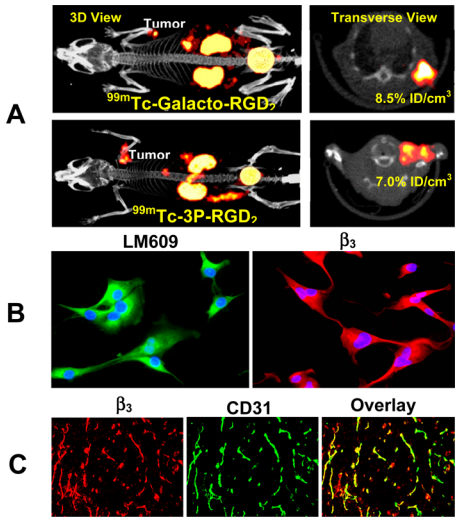

Figure 5. (A) Three-dimensional and transverse views of SPECT/CT images of the athymic nude mice bearing U87MG human glioma xenografts. The animal was administered with ~37 MBq of ^{99m}Tc-3P-RGD$_2$ or ^{99m}Tc-Galacto-RGD$_2$. SPECT/CT study was designed to illustrate their utility for tumor imaging. (B) Representative fluorescence microscopic images of the U87MG primary tumor cells, which were isolated from U87MG glioma tissue and stained with Alexa Fluor 488 conjugated mouse anti-human integrin $\alpha_v\beta_3$ monoclonal antibody LM609 (green) or with rabbit anti-human and murine integrin β_3 antibody (red). Blue color indicates the presence of nuclei stained with DAPI (4′,6-diamidino-2-phenylindole). (C) Selected microscopic images (magnification: 200×) of the tumor slice stained with hamster anti-integrin β_3 (red) and rat anti-CD31 (green) antibodies. Yellow color (red integrin β_3 staining merged with green CD31 staining) indicates the presence of $\alpha_v\beta_3$ on tumor neovasculature.

RGD$_2$ and ^{99m}Tc-3P-RGD$_2$. ^{99m}Tc-3P-RGD$_2$ was used for comparison purpose. Their tumor uptake was ~8.5%ID/cm^3 and ~7.0%ID/cm^3, respectively, on the basis of SPECT quantification. The tumor was clearly visualized by SPECT/CT with excellent contrast with both radiotracers. As expected from biodistribution (Table 1), ^{99m}Tc-Galacto-RGD$_2$ and ^{99m}Tc-3P-RGD$_2$ displayed substantial GI uptake (Figure 5A). The SPECT/CT data clearly showed that both are excellent radiotracers for imaging U87MG gliomas. Figure 5B shows cellular immunostaining data. Figure 5C displays microscopic images of selected tumor slice stained with anti-integrin β_3 (red color) or anti-CD31 (green color) antibody. CD31 was used as a biomarker for tumor blood vessels (mature and neovasculature) and was visualized with FITC (green). Integrin β_3 was visualized with Cy3 (red). Yellow color (overlay between red β_3 staining and green CD31 staining) indicates the presence of integrin $\alpha_v\beta_3$ on tumor neovasculature. It was clear that integrin $\alpha_v\beta_3$ was highly expressed on both U87MG glioma cells and neovasculature, which was in complete agreement with the high uptake of ^{99m}Tc-Galacto-RGD$_2$ in glioma tumors (Table 1).

Metabolism. Metabolism study was performed to show the in vivo stability of ^{99m}Tc-Galacto-RGD$_2$. Figure 6 shows representative radio-HPLC chromatograms of ^{99m}Tc-Galacto-RGD$_2$ in saline before being injected into the animal, in the urine at 30 min p.i. and 120 min p.i., and in the feces at 120 min p.i. There were no metabolites detected in the urine sample over the 2 h study period for ^{99m}Tc-Galacto-RGD$_2$. More than 90% of ^{99m}Tc-Galacto-RGD$_2$ remained intact in the feces sample at 2 h p.i. Its metabolic stability was better than that of ^{99m}Tc-3P-RGD$_2$, only 70% of which remained intact in the feces at 2 h p.i.[31]

DISCUSSION

In this study, we prepared a novel RGD peptide dimer, Galacto-RGD$_2$, which contains a pair of SAA and 1,2,3-triazole groups. A similar approach was used to develop other integrin $\alpha_v\beta_3$-targeted radiotracers,[52,53] such as ^{18}F-RGD-K5, in which 1,2,3-triazole is formed via click reaction to attach the ^{18}F-containing fragment to Galacto-RGD.[52] In Galacto-RGD$_2$, the SAA and 1,2,3-triazole moieties are parts of a linker with two extra PEG$_2$ groups and a glutamic acid residue. Boc-glutamic acid bis-propargyl amide was a key intermediate for synthesis of Galacto-RGD$_2$. It may become an useful building block for click-type of dimerization/multimerization reactions of peptides and other organic molecules via the Cu(I)-catalyzed Huisgen cycloaddition. Click chemistry has proven valuable in development radiopharmaceuticals,[52,54−60] including radiolabeled multimeric cyclic RGD peptides.[55−60]

The integrin $\alpha_v\beta_3$ binding affinity of HYNIC-Galacto-RGD$_2$ (IC_{50} = 20 ± 2 nM) was slightly higher than that of HYNIC-3P-RGD$_2$ (IC_{50} = 32 ± 1 nM), likely due to the rigidity of SAA and 1,2,3-triazole moieties in Galacto-RGD$_2$ as compared to more flexible PEG$_4$ groups in 3P-RGD$_2$. It is important to note that IC_{50} values depends on the radioligand (^{125}I-c(RGDyK) vs ^{125}I-echistatin) and tumor cell lines (U87MG vs MDA-MB-435) used in the competitive assay. Caution should be taken when comparing IC_{50} values of cyclic RGD peptides with those reported in the literature.

^{99m}Tc-Galacto-RGD$_2$ and ^{99m}Tc-3P-RGD$_2$ shared a similar tumor uptake (Figure 4A) despite of slightly higher integrin $\alpha_v\beta_3$ binding affinity of HYNIC-Galacto-RGD$_2$ than that of HYNIC-3P-RGD$_2$. This is most likely related to the fact that both ^{99m}Tc-Galacto-RGD$_2$ and ^{99m}Tc-3P-RGD$_2$ are bivalent in binding to integrin $\alpha_v\beta_3$. As a result, the small difference in their integrin $\alpha_v\beta_3$ binding affinity was not reflected in tumor uptake of their ^{99m}Tc radiotracers. This explanation is also supported by much lower tumor uptake of [^{99m}Tc(HYNIC-RGD$_2$)-(tricine)(TPPTS)] (^{99m}Tc-RGD$_2$), which is only monovalent in binding to integrin $\alpha_v\beta_3$ despite of the presence of two cyclic RGD moieties in RGD$_2$.[31] Bivalency remains the key factor that contributes to the tumor uptake of integrin $\alpha_v\beta_3$-targeted radiotracers.[18]

It must be noted that bivalency is largely dependent on integrin $\alpha_v\beta_3$ receptor density on a specific tissue. In the tumors like xenografted U87MG gliomas, the integrin $\alpha_v\beta_3$ density is high, and the distance between two neighboring integrin $\alpha_v\beta_3$ sites is relatively short. Therefore, it is possible for ^{99m}Tc-Galacto-RGD$_2$ or ^{99m}Tc-3P-RGD$_2$ to be bivalent in binding to integrin $\alpha_v\beta_3$. In most normal organs, however, the integrin $\alpha_v\beta_3$ density is relatively low and the distance between two integrin $\alpha_v\beta_3$ sites is expected to be much longer. In this situation, ^{99m}Tc-Galacto-RGD$_2$ and ^{99m}Tc-3P-RGD$_2$ may not be bivalent in binding to integrin $\alpha_v\beta_3$ expressed on normal tissues.

The major difference between ^{99m}Tc-Galacto-RGD$_2$ and ^{99m}Tc-3P-RGD$_2$ is that two PEG$_4$ groups between the two RGD moieties in 3P-RGD$_2$ are replaced with a pair of SAA, 1,2,3-triazole, and PEG$_2$ moieties. This change resulted in a faster radiotracer washout from tumors (Table 1) and normal organs, most likely due to the improved hydrophilicity.

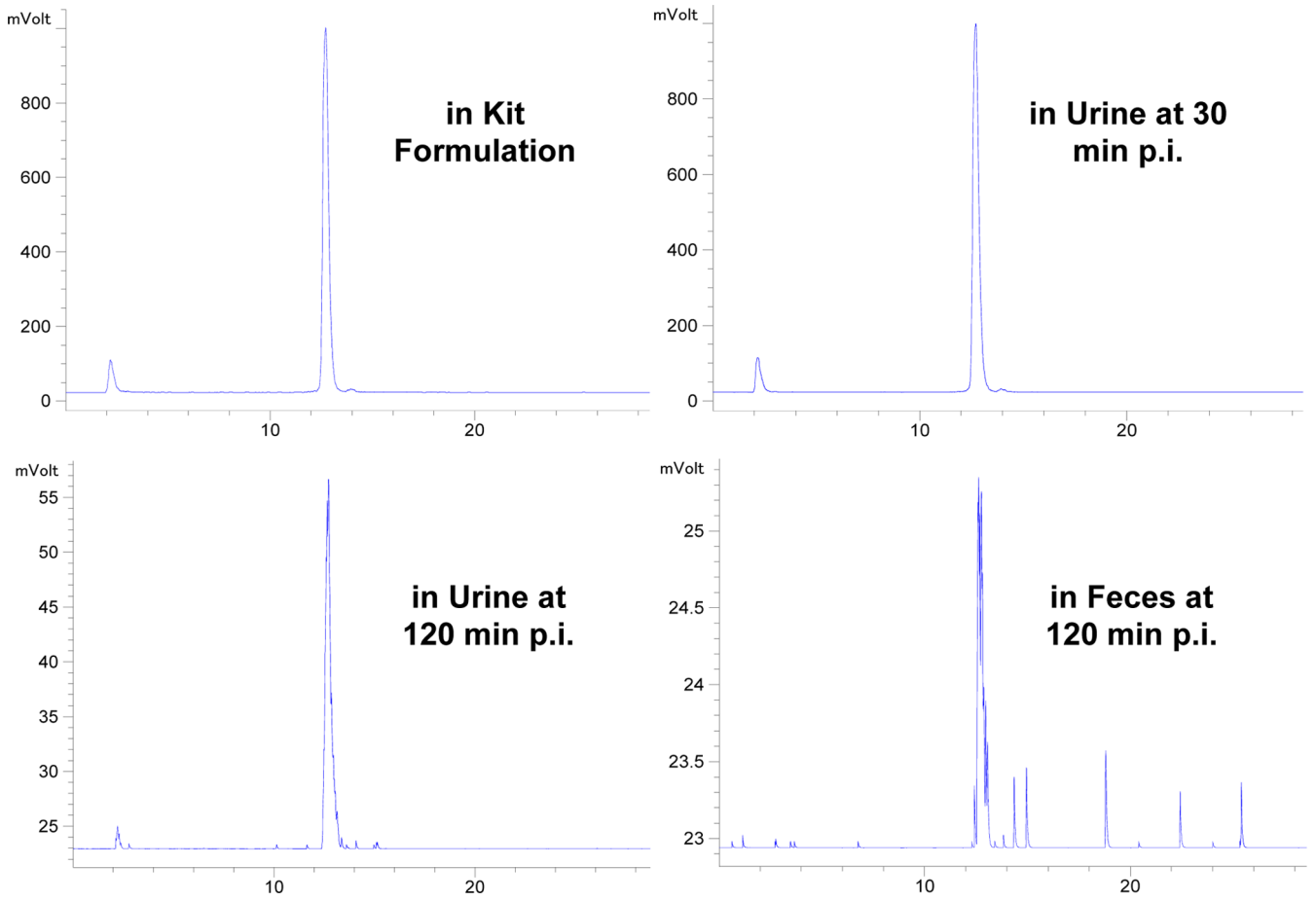

Figure 6. Typical radio-HPLC chromatograms for ^{99m}Tc-Galacto-RGD$_2$ in the saline before injection, in the urine at 30 min p.i. and 120 min p.i., and in the feces at 120 min p.i. Small peaks after the main peak at ~13 min were at the noise level due to the extremely small amount of radioactivity isolated from feces sample for HPLC analysis.

Reduction of radiotracer uptake in the intestines, lungs, and spleen (Figure 4A) is important for diagnosis of tumors in chest and abdominal regions. The integrin $\alpha_v\beta_3$ specificity of ^{99m}Tc-Galacto-RGD$_2$ was demonstrated in the blocking study (Figure 4B). ^{99m}Tc-Galacto-RGD$_2$ was excellent for imaging the xenografted U87MG tumors (Figure 5A). Its high glioma uptake was completely in agreement with the high integrin $\alpha_v\beta_3$ expression on both U87MG glioma cells (Figure 5B) and tumor neovasculature (Figure 5C). ^{99m}Tc-Galacto-RGD$_2$ also had better metabolic stability than ^{99m}Tc-3P-RGD$_2$ during hepatobiliary excretion (Figure 6). All these factors make us to believe that ^{99m}Tc-Galacto-RGD$_2$ has advantages over ^{99m}Tc-3P-RGD$_2$ for imaging tumors and related metastases in the chest and abdominal regions.

In our previous study, it has been clearly demonstrated that many normal organs (particularly intestine, liver, lung, kidneys, and spleen) are integrin $\alpha_v\beta_3$-positive.[38] This is consistent with the reduced uptake of ^{99m}Tc-Galacto-RGD$_2$ in these organs (Figure 4B) in the presence of coinjected excess RGD$_2$. When part of the radiotracer uptake is blocked in integrin $\alpha_v\beta_3$-positive organs, it is not surprising to see elevated blood radioactivity accumulation. However, it does not mean that the radioactivity accumulation in these organs is all integrin $\alpha_v\beta_3$-oriented. For example, the uptake of ^{99m}Tc-Galacto-RGD$_2$ in liver and lung is reduced only by 50%, but its intestine uptake was reduced by ~80% of its origin value. This conclusion is further supported by comparing 60 min biodistribution data of ^{111}In(DOTA-3P-RGD$_2$) and ^{111}In(DOTA-3P-RGK$_2$), which shows very low integrin $\alpha_v\beta_3$ binding affinity (IC_{50} = 715.8 ± 45.1 nM), but still has significant uptake in the intestine, lung, kidneys, and spleen.[39]

CONCLUSION

In this study, we evaluated ^{99m}Tc-Galacto-RGD$_2$ as a new SPECT radiotracer for imaging the xenografted U87MG glioma tumors. We found that ^{99m}Tc-Galacto-RGD$_2$ could be prepared in high specific activity, and was able to maintain its solution stability for >24 h postlabeling. Because of its lower uptake in intestines, lungs, and spleen, ^{99m}Tc-Galacto-RGD$_2$ has advantages over ^{99m}Tc-3P-RGD$_2$ for imaging tumors in the chest and abdominal regions. ^{99m}Tc-Galacto-RGD$_2$ also has a very high metabolic stability. On the basis of results from this and our previous studies,[31−44] we strongly believe that ^{99m}Tc-Galacto-RGD$_2$ is an excellent radiotracer for imaging integrin $\alpha_v\beta_3$-positive tumors and related metastases.

ASSOCIATED CONTENT

Supporting Information

HPLC (Figure SI1), ESI-MS (Figure SI2), and NMR spectral data (Tables SI1 and SI2; Figures SI3−SI8 for DQF-COSY, NOESY, ROESY, TOCSY, HSQC, and HMBC, respectively) to illustrate the purity, composition, and structure of Galacto-RGD$_2$. This material is available free of charge via the Internet at http://pubs.acs.org.

AUTHOR INFORMATION

Corresponding Author

*(S.L.) Mailing address: School of Health Sciences, Purdue University, 550 Stadium Mall Drive, West Lafayette, IN 47907, USA. Phone: 765-494-0236. Fax 765-496-1377. E-mail: liu100@purdue.edu. (A.C.) Mailing address: Peptides International, Inc., 11621 Electron Drive, Louisville, Kentucky 40299, USA. Phone: 502-266-8787. Fax: 502-267-1FAX (1329). E-mail: aczerwinski@pepnet.com.

Notes

The authors declare no competing financial interest.

ACKNOWLEDGMENTS

This work was supported by Purdue University, the Challenge Research Award from Purdue Cancer Center, the Indiana Clinical and Translational Sciences Institute funded in part by Grant Number TR000006 (Clinical and Translational Award) from the National Institutes of Health, National Center for advancing Translational Science, R01 CA115883 (S.L.) from the National Cancer Institute, and KG111333 (Y.Z. and S.L.) from the Susan G. Komen Breast Cancer Foundation.

REFERENCES

(1) Folkman, J. Angiogenesis in cancer, vascular, rheumatoid and other disease. *Nat. Med.* **1995**, *1*, 27−31.

(2) Gasparini, G.; Brooks, P. C.; Biganzoli, E.; Vermeulen, P. B.; Bonoldi, E.; Dirix, L. Y.; Ranieri, G.; Miceli, R.; Cheresh, D. A. Vascular integrin $\alpha_v\beta_3$: a new prognostic indicator in breast cancer. *Clin. Cancer Res.* **1998**, *4*, 2625−2634.

(3) Sengupta, S.; Chattopadhyay, N.; Mitra, A.; Ray, S.; Dasgupta, S.; Chatterjee, A. Role of $\alpha_v\beta_3$ integrin receptors in breast tumor. *J. Exp. Clin. Cancer Res.* **2001**, *20*, 585−590.

(4) Albelda, S. M.; Mette, S. A.; Elder, D. E.; Stewart, R. M.; Damjanovich, L.; Herlyn, M.; Buck, C. A. Integrin distribution in maliganant melanoma: association of the $\alpha_v\beta_3$ subunit with tumor progression. *Cancer Res.* **1990**, *50*, 6757−6764.

(5) Brooks, P. C.; Clark, R. A.; Cheresh, D. A. Requirement of vascular integrin $\alpha_v\beta_3$ for angiogenesis. *Science* **1994**, *264*, 569−571.

(6) Hwang, R.; Varner, J. V. The role of integrins in tumor angiogenesis. *Hematol. Oncol. Clin. North Am.* **2004**, *18*, 991−1006.

(7) Bello, L.; Francolini, M.; Marthyn, P.; Zhang, J. P.; Carroll, R. S.; Nikas, D. C.; Strasser, J. F.; Villani, R.; Cheresh, D. A.; Black, P. M. $\alpha_v\beta_3$ and $\alpha_v\beta_5$ integrin expression in glioma periphery. *Neurosurgery* **2001**, *49*, 380−389.

(8) Jin, H.; Varner, J. Integrins: roles in cancer development and as treatment targets. *Br. J. Cancer* **2004**, *90*, 561−565.

(9) Zitzmann, S.; Ehemann, V.; Schwab, M. Arginine-Glycine-Aspartic acid (RGD)-peptide binds to both tumor and tumor endothelial cells in vivo. *Cancer Res.* **2002**, *62*, 5139−5143.

(10) D'Andrea, L. D.; Del Gatto, A.; Pedone, C.; Benedetti, E. Peptide-based molecules in angiogenesis. *Chem. Biol. Drug Des.* **2006**, *67*, 115−126.

(11) Meyer, A.; Auremheimer, J.; Modlinger, A.; Kessler, H. Targeting RGD recognizing integrins: drug development, biomaterial research, tumor imaging and targeting. *Curr. Pharm. Des.* **2006**, *12*, 2723−2747.

(12) Weber, W. A.; Haubner, R.; Vabuliene, E.; Kuhnast, B.; Webster, H. J.; Schwaiger, M. Tumor angiogenesis targeting using imaging agents. *Q. J. Nucl. Med.* **2001**, *45*, 179−182.

(13) Haubner, R.; Wester, H. R. Radiolabeled tracers for imaging of tumor angiogenesis and evaluation of anti-angiogenic therapies. *Curr. Pharm. Des.* **2004**, *10*, 1439−1455.

(14) Liu, S. Radiolabeled multimeric cyclic RGD peptides as integrin $\alpha_v\beta_3$-targeted radiotracers for tumor imaging. *Mol. Pharmaceutics* **2006**, *3*, 472−487.

(15) Cai, W.; Chen, X. Multimodality imaging of tumor angiogenesis. *J. Nucl. Med.* **2008**, *49*, 113S−128S.

(16) Liu, S. Radiolabeled RGD peptides as integrin $\alpha_v\beta_3$-targeted radiotracers: maximizing binding affinity via bivalency. *Bioconjugate Chem.* **2009**, *20*, 2199−2213.

(17) Ingrid Dijkgraaf, I.; Boerman, O. C. Molecular imaging of angiogenesis with SPECT. *Eur. J. Nucl. Med. Mol. Imaging* **2010**, *37* (Suppl 1), S104−S113.

(18) Tateishi, U.; Oka, T.; Inoue, T. Radiolabeled RGD Peptides as Integrin alpha(v)beta3−targeted PET Tracers. *Curr. Med. Chem.* **2012**, *19*, 3301−3309.

(19) Haubner, R.; Wester, H. J.; Weber, W. A.; Mang, C.; Ziegler, S. I.; Goodman, S. L.; Senekowitsch-Schmidtke, R.; Kessler, H.; Schwaiger, M. Noninvasive imaging of $\alpha_v\beta_3$ integrin expression using ^{18}F-labeled RGD-containing glycopeptide and positron emission tomography. *Cancer Res.* **2001**, *61*, 1781−1785.

(20) Nwe, K.; Kim, Y.-S.; Milenic, D. E.; Baidoo, K. E.; Brechbiel, M. W. ^{111}In- and ^{203}Pb-labeled cyclic arginine-glycine-aspartic acid peptide conjugate as an $\alpha_v\beta_3$ integrin-binding radiotracer. *J. Labelled Compd. Radiopharm.* **2012**, *55*, 423−426.

(21) Pohle, K.; Notni, J.; Bussemer, J.; Kessler, H.; Schwaiger, M.; Beer, A. J. ^{68}Ga-NODAGA-RGD is a suitable substitute for ^{18}F-Galacto-RGD and can be produced with high specific activity in a cGMP/GRP compliant automated process. *Nucl. Med. Biol.* **2012**, *39*, 777−784.

(22) Li, Y.; Guo, J.; Tang, S.; Lang, L.; Chen, X.; Perrin, D. M. One-step and one-pot-two-step radiosynthesis of cyclo-RGD-^{18}F-aryltrifluoroborate conjugates for functional imaging. *Am. J. Nucl. Med. Mol. Imaging* **2013**, *3*, 44−56.

(23) Tsiapa, I.; Loudos, G.; Varvarigou, A.; Fragogeorgi, E.; Psimadas, D.; Tsotakos, T.; Xanthopoulos, S.; Mihailidis, D.; Bouziotis, P.; Nikiforidis, G. C.; Kagadis, G. C. Biological evaluation of an ornithine-modified ^{99m}Tc-labeled RGD peptide as an angiogenesis imaging agent. *Nucl. Med. Biol.* **2013**, *40*, 262−272.

(24) Wu, Y.; Zhang, X.; Xiong, Z.; Cheng, Z.; Fisher, D. R.; Liu, S.; Gambhir, S. S.; Chen, X. MicroPET imaging of glioma integrin $\alpha_v\beta_3$ expression using ^{64}Cu-labeled tetrameric RGD peptide. *J. Nucl. Med.* **2005**, *46*, 1707−1718.

(25) Wu, Z.; Li, Z. B.; Chen, K.; Cai, W.; He, L.; Chin, F. T.; Li, F.; Chen, X. MicroPET of tumor integrin $\alpha_v\beta_3$ expression using ^{18}F-labeled PEGylated tetrameric RGD peptide (^{18}F-FPRGD4). *J. Nucl. Med.* **2007**, *48*, 1536−1544.

(26) Liu, Z.; Niu, G.; Shi, J.; Liu, S.; Wang, F.; Chen, X. ^{68}Ga-labeled cyclic RGD dimers with Gly_3 and PEG_4 linkers: promising agents for tumor integrin $\alpha_v\beta_3$ PET imaging. *Eur. J. Nucl. Med. Mol. Imaging* **2009**, *36*, 947−957.

(27) Liu, Z.; Liu, S.; Wang, F.; Chen, X. Noninvasive imaging of tumor integrin expression using ^{18}F-labeled RGD dimer peptide with PEG_4 linkers. *Eur. J. Nucl. Med. Mol. Imaging* **2009**, *36*, 1296−1307.

(28) Dijkgraaf, I.; Liu, S.; Kruijtzer, J. A.; Soede, A. C.; Oyen, W. J.; Liskamp, R. M.; Corstens, F. H.; Boerman, O. C. Effect of linker variation on the in vitro and in vivo characteristics of an ^{111}In-labeled RGD Peptide. *Nucl. Med. Biol.* **2007**, *34*, 29−35.

(29) Dijkgraaf, I.; Kruijtzer, J. A.; Liu, S.; Soede, A. C.; Oyen, W. J.; Corstens, F. H.; Liskamp, R. M.; Boerman, O. C. Improved targeting of the $\alpha_v\beta_3$ integrin by multimerization of RGD peptides. *Eur. J. Nucl. Med. Mol. Imaging* **2007**, *34*, 267−273.

(30) Liu, S.; Edwards, D. S.; Ziegler, M. C.; Harris, A. R.; Hemingway, S. J.; Barrett, J. A. ^{99m}Tc-Labeling of a hydrazinonicotinamide-conjugated vitronectin receptor antagonist. *Bioconjugate Chem.* **2001**, *12*, 624−629.

(31) Wang, L.; Shi, J.; Kim, Y. S.; Zhai, S.; Jia, B.; Zhao, H.; Liu, Z.; Wang, F.; Chen, X.; Liu, S. Improving tumor targeting capability and pharmacokinetics of ^{99m}Tc-labeled cyclic RGD dimers with PEG_4 linkers. *Mol. Pharmaceutics* **2009**, *6*, 231−245.

(32) Shi, J.; Wang, L.; Kim, Y. S.; Zhai, S.; Liu, Z.; Chen, X.; Liu, S. Improving tumor uptake and excretion kinetics of ^{99m}Tc-labeled cyclic Arginine-Glycine-Aspartic (RGD) dimers with triglycine linkers. *J. Med. Chem.* **2008**, *51*, 7980−7990.

(33) Shi, J.; Wang, L.; Kim, Y. S.; Zhai, S.; Jia, B.; Wang, F.; Liu, S. ^{99m}TcO(MAG$_2$-3G$_3$-dimer): A new integrin $\alpha_v\beta_3$-targeted radiotracer with high tumor uptake and favorable pharmacokinetics. *Eur. J. Nucl. Med. Mol. Imaging* **2009**, *36*, 1874−1884.
(34) Shi, J.; Kim, Y. S.; Zhai, S.; Liu, Z.; Chen, X.; Liu, S. Improving tumor uptake and pharmacokinetics of ^{64}Cu-labeled cyclic RGD dimers with triglycine and PEG$_4$ linkers. *Bioconjugate Chem.* **2009**, *20*, 750−759.
(35) Shi, J.; Kim, Y. S.; Chakraborty, S.; Jia, B.; Wang, F.; Liu, S. 2-Mercaptoacetylglycylglycyl (MAG$_2$) as a bifunctional chelator for ^{99m}Tc-labeling of cyclic RGD dimers: effects of technetium chelate on tumor uptake and pharmacokinetics. *Bioconjugate Chem.* **2009**, *20*, 1559−1568.
(36) Chakraborty, S.; Liu, S.; Kim, Y. S.; Shi, J.; Zhou, Y.; Wang, F. Evaluation of ^{111}In-labeled cyclic RGD peptides: tetrameric not tetravalent. *Bioconjugate Chem.* **2011**, *21*, 969−978.
(37) Zhou, Y.; Kim, Y. S.; Chakraborty, S.; Shi, J.; Gao, H.; Liu, S. ^{99m}Tc-Labeled cyclic RGD peptides for noninvasive monitoring of tumor integrin $\alpha_v\beta_3$ expression. *Mol. Imaging* **2011**, *10*, 386−97.
(38) Shi, J.; Zhou, Y.; Chakraborty, S.; Kim, Y. S.; Jia, B.; Wang, F.; Liu, S. Evaluation of ^{111}In-labeled cyclic RGD peptides: effects of peptide and PEG$_4$ multiplicity on their tumor uptake, excretion kinetics and metabolic stability. *Theranostics* **2011**, *1*, 322−340.
(39) Shi, J.; Jia, B.; Kim, Y. S.; Chakraborty, S.; Zhou, Y.; Wang, F.; Liu, S. Impact of bifunctional chelators on biological properties of ^{111}In-labeled cyclic peptide RGD dimers. *Amino Acids* **2011**, *41*, 1059−1070.
(40) Jia, B.; Liu, Z.; Zhu, Z.; Shi, J.; Jin, X.; Zhao, H.; Li, F.; Liu, S.; Wang, F. Blood clearance kinetics, biodistribution and radiation dosimetry of a kit-formulated integrin $\alpha_v\beta_3$-selective radiotracer ^{99m}Tc-3PRGD$_2$ in non-human primates. *Mol. Imaging Biol.* **2011**, *13*, 730−736.
(41) Zhou, Y.; Kim, Y. S.; Lu, X.; Liu, S. Evaluation of ^{99m}Tc-labeled cyclic RGD dimers: impact of cyclic RGD peptides and ^{99m}Tc chelates on biological properties. *Bioconjugate Chem.* **2012**, *23*, 586−595.
(42) Zhou, Y.; Kim, Y. S.; Chakraborty, S.; Shi, J.; Gao, H.; Liu, S. ^{99m}Tc-labeled cyclic RGD peptides for noninvasive monitoring of tumor integrin $\alpha_v\beta_3$ expression. *Mol. Imaging* **2011**, *10*, 386−397.
(43) Shao, G.; Zhou, Y.; Liu, S. Monitoring glioma growth and tumor necrosis with u-SPECT-II/CT for by targeting integrin $\alpha_v\beta_3$. *Mol. Imaging* **2013**, *12*, 39−48.
(44) Zhou, Y.; Shao, G.; Liu, S. Imaging breast cancer lung metastasis by u-SPECT-II/CT with an integrin $\alpha_v\beta_3$-targeted radiotracer ^{99m}Tc-3P-RGD$_2$. *Theranostics* **2012**, *2*, 577−587.
(45) Ma, Q.; Ji, B.; Jia, B.; Gao, S.; Ji, T.; Wang, X.; Han, Z.; Zhao, G. Differential diagnosis of solitary pulmonary nodules using ^{99m}Tc-3P4-RGD2 scintigraphy. *Eur. J. Nucl. Med. Mol. Imaging* **2011**, *38*, 2145−52.
(46) Zhu, Z.; Miao, W.; Li, Q.; Dai, H.; Ma, Q.; Wang, F.; Yang, A.; Jia, B.; Jing, X.; Liu, S.; Shi, J.; Liu, Z.; Zhao, Z.; Li, F. ^{99m}Tc-3PRGD2 for integrin receptor imaging of lung cancer: a multicenter study. *J. Nucl. Med.* **2012**, *53*, 716−22.
(47) Haubner, R.; Kuhnast, B.; Mang, C.; Weber, W. A.; Kessler, H.; Wester, H. J.; Schwaiger, M. [^{18}F]Galacto-RGD: Synthesis, Metabolic Stability, and Radiation Dose Estimates. *Bioconjugate Chem.* **2004**, *15*, 61−69.
(48) Walsh, J. C.; Kolb, H. C. Applications of click chemistry in radiopharmaceutical development. *Chimia* **2010**, *64*, 29−33.
(49) Harris, T. D.; Sworin, M.; Williams, N.; Rajopadhye, M.; Damphousse, P. R.; Glowacka, D.; Poirier, M. J.; Yu, K. Synthesis of stable hydrazones of a hydrazinonicotinyl-modified peptide for the preparation of ^{99m}Tc-labeled radiopharmaceuticals. *Bioconjugate Chem.* **1998**, *10*, 808−814.
(50) Shioiri, T.; Yamada, S. Amino acids and peptides. IX. Phosphorus in organic synthesis. IV. Diphenyl phosphorazidate. A new convenient reagent for the peptide synthesis. *Chem. Pharm. Bull. (Tokyo)* **1974**, *22*, 849−854.
(51) Shioiri, T.; Yamada, S. (1974) Amino acids and peptides. X. Phosphorus in organic synthesis. V. On the mechanism for the peptide synthesis by diphenyl phosphorazidate. *Chem. Pharm. Bull. Chem. Pharm. Bull. (Tokyo)* **1974**, *22*, 855−858.
(52) Efthymiou, T.; Gong, W.; Desaulniers, J. P. Chemical architecture and applications of nucleic acid derivatives containing 1,2,3-triazole functionalities synthesized via click chemistry. *Molecules* **2012**, *17*, 12665−12703.
(53) Doss, M.; Kolb, H. C.; Zhang, J. J.; Bélanger, M. J.; Stubbs, J. B.; Stabin, M. G.; Hostetler, E. D.; Alpaugh, R. K.; Mehren, M.; Walsh, J. C.; Haka, M.; Mocharla, V. P.; Yu, J. Q. Biodistribution and radiation dosimetry of the integrin marker ^{18}F-RGD-K5 determined from whole-body PET/CT in monkeys and humans. *J. Nucl. Med.* **2012**, *53*, 787−795.
(54) Mamat, C.; Ramenda, T.; Wuest, F. R. Recent applications of click chemistry for the synthesis of radiotracers for molecular imaging. *Mini-Rev. Org. Chem.* **2009**, *6*, 21−34.
(55) Best, M. D. Click chemistry and bioorthogonal reactions: unprecedented selectivity in the labeling of biological molecules. *Biochemistry* **2009**, *48*, 6571−6584.
(56) Wängler, C.; Maschauer, S.; Prante, O.; Schafer, M.; Schirrmacher, R.; Bartenstein, P.; Eisenhut, M.; Wängler, B. Multimerization of cRGD peptides by click chemistry: synthetic strategies, chemical limitations, and influence on biological properties. *ChemBioChem* **2010**, *11*, 2168−2181.
(57) Galibert, M.; Sancey, L.; Renaudet, O.; Coll, J. L.; Dumy, P.; Boturyn, D. Application of click-click chemistry to the synthesis of new multivalent RGD conjugates. *Org. Biomol. Chem.* **2010**, *8*, 5133−5138.
(58) Colombo, M.; Bianchi, A. Click chemistry for the synthesis of RGD-containing integrin ligands. *Molecules* **2010**, *15*, 178−197.
(59) Trabocchi, A.; Menchi, G.; Cini, N.; Bianchini, F.; Raspanti, S.; Bottoncetti, A.; Pupi, A.; Calorini, L.; Guarna, A. Click-chemistry-derived triazole ligands of arginine-glycine-aspartate (RGD) integrins with a broad capacity to inhibit adhesion of melanoma cells and both in vitro and in vivo angiogenesis. *J. Med. Chem.* **2010**, *53*, 7119−7128.
(60) Kowalczyk, W.; Mascaraque, A.; Sanchez-Navarro, M.; Rojo, J.; Andreu, D. Convergent synthesis of glycodendropeptides by click chemistry approaches. *Eur. J. Org. Chem.* **2012**, 4565−4573.

NOTE ADDED AFTER ASAP PUBLICATION

This paper was published ASAP on August 6, 2013. Chart I has been revised. The corrected version was reposted on August 9, 2013.